Human Molecular Genetics, 2016, Vol. 25, No. 16 3500–3514

doi: 10.1093/hmg/ddw193
Advance Access Publication Date: 29 June 2016
Original Article

ORIGINAL ARTICLE

The K153Del PRPH2 mutation differentially impacts photoreceptor structure and function

Dibyendu Chakraborty[1], Shannon M. Conley[1], Rahel Zulliger[2] and Muna I. Naash[2,*]

[1]Department of Cell Biology, University of Oklahoma Health Sciences Center, Oklahoma City, OK, USA and [2]Department of Biomedical Engineering, University of Houston, Houston, TX, USA.

*To whom correspondence should be addressed at: Department of Biomedical Engineering, University of Houston, 3517 Cullen Blvd. Room 2011, Houston, TX 77204-5060, USA. Tel: +713-743-1651; Email: mnaash@central.uh.edu

Abstract

Peripherin 2 (Prph2) is a photoreceptor tetraspanin, and deletion of codon 153 (K153Δ) leads to retinitis pigmentosa, pattern dystrophy, and fundus flavimaculatus in the same family. To study this variability, we generated a K153Δ-*Prph2* knockin mouse. K153Δ-Prph2 cannot form the complexes required for outer segment formation, and in cones cannot interact with its binding partner rod outer segment membrane protein 1. K153Δ causes dominant defects in rod and cone function; however, rod but not cone ultrastructure is improved by the presence of K153Δ-Prph2. Likewise, supplementation of K153Δ heterozygotes with WT-Prph2 results in structural but not functional improvements. These results support the idea that mutations may differentially affect Prph2's role as a structural component, and its role as a functional protein key for organizing membrane domains for cellular signalling. These roles may be different in rods and cones, thus contributing to the phenotypic heterogeneity that characterizes diseases associated with *Prph2* mutations.

Introduction

Peripherin 2 (Prph2 also/previously known as retinal degeneration slow/RDS) is a 346 amino acid glycoprotein with four transmembrane domains (1). Over 151 mutations in the Prph2 gene have been implicated in the pathogenesis of several varieties of human retinal degenerative diseases including autosomal dominant retinitis pigmentosa (RP) and various forms of macular dystrophy (Human Gene Mutation Database http://www.hgmd.cf.ac.uk/ac/gene.php?gene=PRPH2, last accessed 24 June 2016). Prph2 is a structural protein essential for the formation of rod and cone outer segments (OSs), and in its absence photoreceptors terminate at the connecting cilium (2). The Prph2 protein contains a highly conserved large intradiscal loop, called D2, of approximately 150 amino acids. The D2 loop plays an important role in the Prph2 complex assembly necessary for disc formation and stabilization (3–7), and many disease-causing mutations are located in the D2 loop (8,9).

Prph2 forms non-covalent homo- and hetero-tetramers with its non-glycosylated homologue, rod outer segment membrane protein 1 (ROM1) (5,6), another member of the tetraspanin family also localized to the disc rim region of both photoreceptor cell types. These tetramers are assembled in the inner segment and then traffic to the rim region of the OS where they further complex through intermolecular disulphide bonds to form octamers and higher-order oligomers (4). These disulphide linked complexes are essential (5,7); when the cysteine that mediates the covalent linkage (C150) is ablated, OSs fail to form (3,10). Though ROM1 forms covalent linkages and is found in the octameric complexes; it does not participate in higher-order oligomers (3,4). Elimination of Rom1 (*Rom1*$^{-/-}$) leads to much

Received: March 3, 2016. **Revised:** May 18, 2016. **Accepted:** June 16, 2016

more minor phenotypes (11) than the elimination of Prph2 (2); it is thought to play an ancillary or regulatory role rather than a key structural one. However, studies evaluating Rom1 focused on rods (11), so it is not clear what its role is in cones. In addition, *ROM1* mutations have recently been shown to act as genetic modifiers in some cases of *Prph2*-associated macular disease (12), suggesting that ROM1 should not be overlooked.

One of our goals has been to explore the mechanisms underlying the widely varying phenotypes associated with *Prph2* mutations, and here we focus on a three base pair deletion mutation which eliminates lysine at position 153 or 154 in the Prph2 D2 loop. This mutation, which is referred to as K153Δ, produces clinically variable phenotypes in patients even in the same family (13). Patient phenotypes range from the largely rod-dominant RP, to more macular phenotypes such as pattern dystrophy (PD) and fundus flavimaculatus. This high degree of phenotypic heterogeneity and variation in age-of-onset, severity and penetrance is common to many *Prph2* disease mutations. This variety complicates the study of disease mechanisms and the development of therapeutics, and makes studies evaluating disease mechanisms essential to progress in the field. Here, we generate a K153Δ *Prph2* knockin mouse model to evaluate the molecular disease mechanisms associated with mutant Prph2, in order to facilitate understanding of the human disease.

We show exciting new data suggesting that defects in Prph2/Rom1 complex assembly underlie rod versus cone differences in *Prph2*-associated pathologies. We find that K153Δ Prph2 cannot form the intermolecular disulphide linkages or higher-order Prph2 complexes known to be required for OS formation, and that in cones but not rods this leads to an elimination of Prph2/Rom1 binding. These divergent defects in complex assembly in rods versus cones also affect disease phenotypes. In the presence of WT Prph2 (as in patients), the K153Δ allele causes dominant defects in rod and cone function. However, these functional defects do not correlate with structural outcomes; rod but not cone ultrastructure is actually improved by the presence of one allele of K153Δ *Prph2* (compared to $Prph2^{+/-}$), suggesting a disconnect between the two cell-types in terms of the structural and functional roles of Prph2, and signifying that mutations can impact one but not the other.

Results

K153Δ Prph2is expressed in knockin retinas

We generated a knockin mouse line carrying the three base pair deletion which leads to the K153Δmutation (abbreviated KΔ) in the native *Prph2* locus (Fig. 1A). The heterozygous ($Prph2^{K\Delta/+}$) mice genetically mimic the human patients (who carry one wild-type [WT] and one mutant allele), but we also evaluated homozygous $Prph2^{K\Delta/K\Delta}$ retinas to study the mutant protein, since it cannot be distinguished from the WT Prph2 using antibodies. Controls included WT animals and those heterozygous or homozygous for the naturally occurring Prph2 null allele (called *rds*, and previously referred to as *rds/rds*, *rd2*, and $rds^{-/-}$) (2,14). For simplicity's sake, we will refer to these lines as $Prph2^{+/-}$ and $Prph2^{-/-}$, respectively. The $Prph2^{+/-}$ is an especially useful model as it exhibits a well-characterized haploinsufficiency RP phenotype (14,15).

At postnatal day (P) 30, levels of *Prph2* transcript (measured by qRT-PCR) in $Prph2^{K\Delta/K\Delta}$ retinas were not significantly different from WT (Fig. 1B), confirming that the knockin allele was transcribed normally. We next measured Prph2 and Rom1 protein levels densitometrically. Levels are plotted for each genotype as the percent of Prph2/Rom1 compared to WT (after normalizing to actin). We found that Prph2 protein levels in $Prph2^{K\Delta/K\Delta}$ were significantly reduced to ~20% of WT (Fig. 1C, $^{***}P < 0.001$ by 1-way ANOVA with Bonferroni's post-hoc comparison), suggesting that the K153Δ mutation rendered the protein unstable. Prph2 levels in $Prph2^{K\Delta/+}$ were also reduced to ~80% of WT, though the difference was not statistically significant, and mean Prph2 levels were higher than those found in the $Prph2^{+/-}$ (~60% of WT). Rom1 levels paralleled these changes in Prph2, and were reduced in both the $Prph2^{K\Delta/+}$ (to ~75% of WT) and the $Prph2^{K\Delta/K\Delta}$ retina (to ~15% of WT, Fig. 1D).

K153Δ Prph2 leads to significant reductions in rod structure and function

In some patients, K153Δis associated with RP (13). Therefore to evaluate rod function, we performed full-field scotopic electroretinography (ERG). Figure 1E shows representative ERG waveforms at P30 with quantification of maximum amplitudes at P30, P180 and P365 (Fig. 1F–H, respectively). A significant (~63%) reduction in maximum scotopic a-wave was observed in $Prph2^{K\Delta/+}$ versus WT at P30 (Fig. 1F), a defect also reflected in maximum scotopic b-wave amplitudes. This decrease worsened at P180 and P365 (Fig. 1G–H). At early time-points, scotopic ERG amplitudes were slightly worse in $Prph2^{K\Delta/+}$ compared to $Prph2^{+/-}$ (Fig. 1F), and though statistical significance was lost at later ages, mean scotopic ERG values continued to be lower in $Prph2^{K\Delta/+}$ compared to $Prph2^{+/-}$ at all time-points tested. When examined in light of our observation that total Prph2 protein levels in the $Prph2^{K\Delta/+}$ were ~80% of WT, an amount of Prph2 that has previously been shown to rescue the $Prph2^{+/-}$ phenotype (16), this suggests that the K153Δ Prph2 mutant protein is largely non-functional in rods, and may in fact have some dominant-negative effect. Scotopic ERG amplitudes in $Prph2^{K\Delta/K\Delta}$ were very low and not significantly different from those in the $Prph2^{-/-}$ retinas at P30 (Fig. 1F), though waveforms show some signal when compared to $Prph2^{-/-}$ (Fig. 1E). Given the virtually undetectable nature of scotopic responses in $Prph2^{K\Delta/K\Delta}$ and $Prph2^{-/-}$ at P30 these animals were not evaluated at later time-points.

We next assessed the effects of the K153Δ allele on rod structure. As shown in light micrographs, at P30, overall retinal lamination in animals carrying the K153Δ allele was normal (Fig. 2A, top). Likewise, outer nuclear layer (ONL) thickness (Fig. 2B) was not changed between $Prph2^{+/-}$, $Prph2^{K\Delta/+}$, and WT. However, on the ultrastructural level, substantial differences were seen between them (Fig. 2a, bottom). Rod OSs in the $Prph2^{+/-}$ consist of large abnormal whorls (Fig. 2A, arrows), and overall length is substantially decreased from the WT (Fig. 2C and (15,17)). However, although the thickness of the OS layer (Fig. 2C) in the $Prph2^{K\Delta/+}$ is comparable to $Prph2^{+/-}$, the ultrastructure of OSs in the $Prph2^{K\Delta/+}$ is improved. OSs in the $Prph2^{K\Delta/+}$ exhibit better disc stacking (Fig. 2a, bottom, arrowheads) and alignment (albeit not to the level of the WT), and rarely display the large whorls characteristic of the $Prph2^{+/-}$. This improvement in OS stacking is reflected in higher mean rhodopsin levels in the $Prph2^{K\Delta/+}$ compared to $Prph2^{+/-}$ ($^{***}P < 0.001$ by 1-way ANOVA, Fig. 2D). As expected due to OS shortening, rhodopsin levels in the $Prph2^{+/-}$ are ~33% of WT, while those in the $Prph2^{K\Delta/+}$ are ~59% of WT. A small subset of WT, $Prph2^{+/-}$, and $Prph2^{K\Delta/+}$ animals was aged to P180, and at this age, ONL thickness appears to be reduced in $Prph2^{K\Delta/+}$ versus $Prph2^{+/-}$, but OS ultrastructure remains

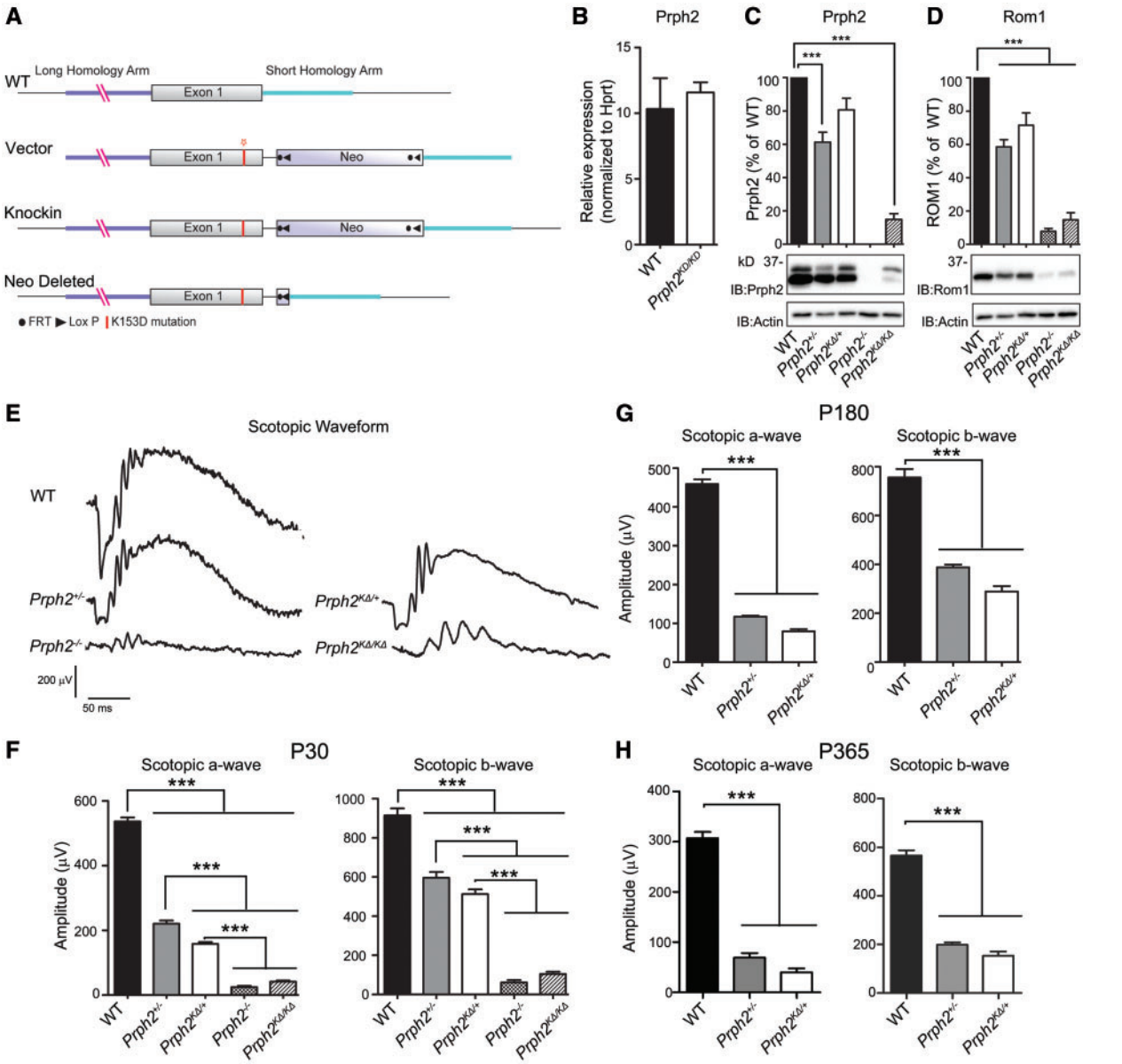

Figure 1. K153Δ message is normal but protein level is reduced. **(A)** Diagram of the K153ΔPrph2 knockin strategy. **(B)** Total retinal RNA was isolated at P30 and subjected to qRT-PCR for *Prph2* and the housekeeping gene *Hprt*, $n = 4$–5 retinas/group. **(C)** Levels of Prph2 and Rom1 protein were analyzed by reducing SDS-PAGE/western blot from retinal extracts of indicated genotypes. Band intensities were normalized to actin, then presented as percent of WT. $n = 4$–5 retinas/group. **(E)** Full-field ERGs were recorded under scotopic conditions. Representative P30 ERG waveforms are shown from all listed genotypes. **(F–H)** Mean (±SEM) maximum scotopic A- and B-waves waves are plotted for recordings at P30, P180, and P365 in **F–H**, respectively. $n = 5$–10 mice per genotype. ***$P < 0.001$ by one-way ANOVA with Bonferroni's post-hoc comparison, graphs shown mean ±SEM.

improved (Fig. 2E). This improvement in disc stacking and alignment is widespread in the $Prph2^{K\Delta/+}$as seen in lower magnification EM (Supplementary Material, Fig. S1).

No OSs are formed in the $Prph2^{-/-}$, and this is largely the case in the $Prph2^{K\Delta/K\Delta}$, however, we infrequently see whorl-shaped membranous OSs similar in morphology to those in the $Prph2^{+/-}$ but smaller (Fig. 2a, bottom, white arrow, and black arrows in Supplementary Material, Fig. S1). This suggests that K153Δ Prph2 by itself can initiate disc rim formation but cannot support proper growth and maintenance of OSs in the absence of WT Prph2. It is likely that this small membranous structure provides a place for rhodopsin which is reflected in the increased in rhodopsin levels in the$Prph2^{K\Delta/K\Delta}$ (~15% of WT) compared to the$Prph2^{-/-}$(~6% of WT) (Fig. 2D). Combined these data suggest that while the K153Δ Prph2 protein present in the $Prph2^{K\Delta/+}$may be enough to mediate improved disc stacking/alignment, it is not fully functional and thus cannot support lengthening of the OS or improvements in rod function (compared to the $Prph2^{+/-}$).

Expression of K153Δ Prph2 affects cone function

Previous studies from our lab (3,18) showed that Prph2 plays a differential role in rod versus cone photoreceptors, a topic of particular interest for the K153Δ mutation, given its widely varying patient phenotypes. To evaluate the effect of K153Δ Prph2 in

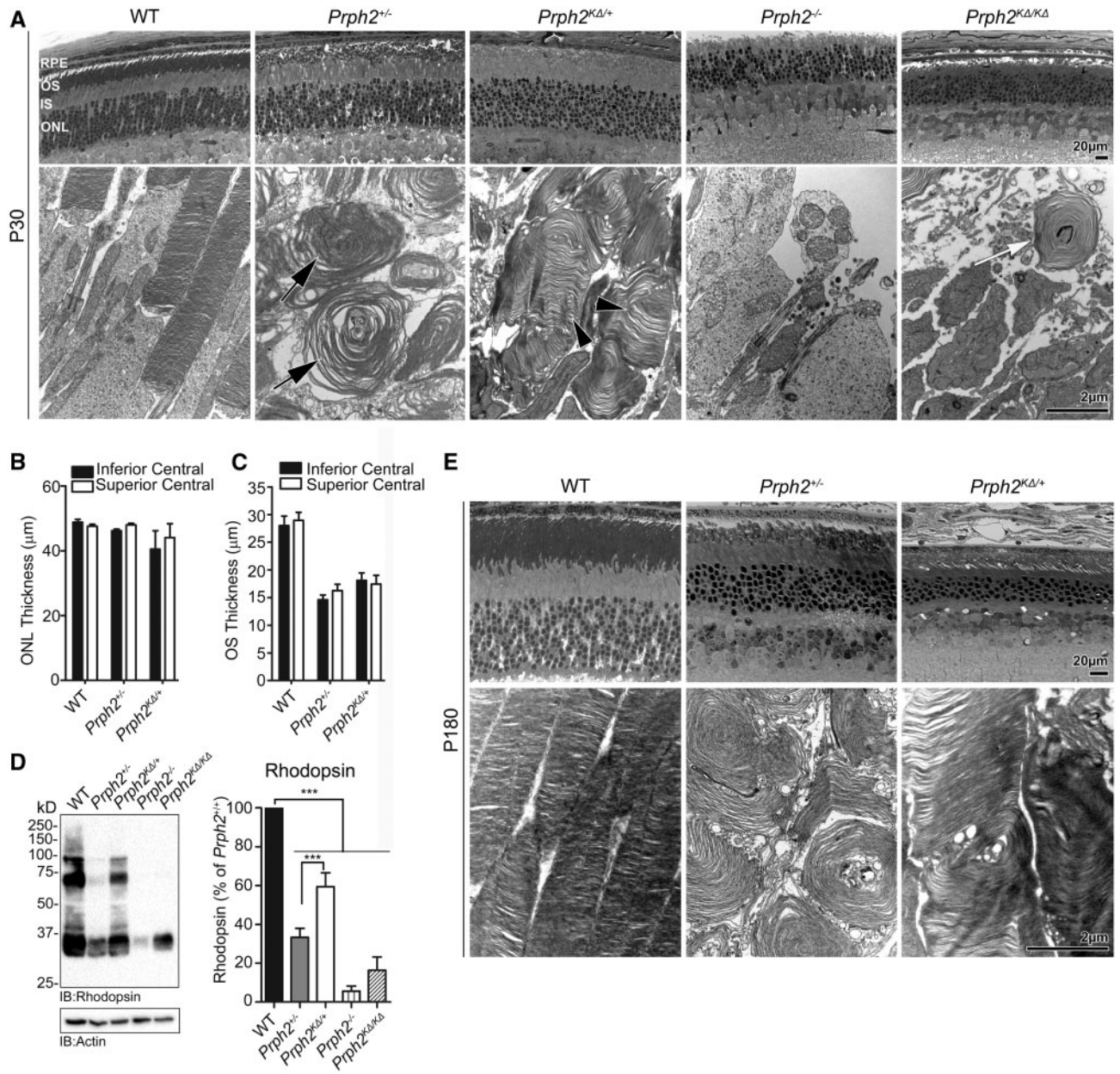

Figure 2. K153ΔPrph2 is unable to support normal OS formation. **(A)** Shown are representative light microscopy (top) and transmission EM (bottom) from the indicated genotypes at P30. Black arrow indicate whorl OSs characteristic of the *Prph2*$^{+/-}$, arrowheads indicate improved disc stacking and alignment in the *Prph2*$^{K\Delta/+}$ while white arrows indicate the highly malformed OSs of the *Prph2*$^{K\Delta/K\Delta}$. **(B–C)** ONL thickness (**B**) and OS length (**C**) was measured from the superior and inferior central retina and plotted as a mean ± SEM, $n = 3$–5 eyes/genotype. **(D)** Rhodopsin protein levels were assessed by SDS-PAGE/western blot and quantified, plotted are means ±SEM, $n = 3$–7 retinas/genotype, ***$P < 0.001$ by one-way ANOVA with Bonferroni's post-hoc comparison. **(E)** Shown are representative light microscopy (top) and transmission EM (bottom) from the indicated genotypes at P180. Scale bars are 20 μm (light images) and 2 μm (EM images). RPE: retinal pigment epithelium, OS: outer segment, IS: inner segment, ONL: outer nuclear layer.

cone photoreceptors, we performed full-field photopic ERG from light-adapted animals. Photopic ERG waveforms were recorded at P30 with white light (Fig. 3A) and maximum photopic b-wave amplitudes were quantified at P30, P180, and P365 (Fig. 3B–D, respectively). At P30, photopic recordings under white light are unaffected in the *Prph2*$^{+/-}$, consistent with it being a model for Prph2-associated RP, in which decreases in cone function are late-onset (15). However, photopic ERG amplitudes at P30 under both white light and short (UV) or medium (green) wavelength light, were significantly reduced in *Prph2*$^{K\Delta/+}$ compared to *Prph2*$^{+/-}$ and WT (Fig. 3B); though no differences in response pattern were observed between UV and green cones. This striking deleterious effect of the K153Δ allele on cone function was also evident at older ages (Fig. 3C–D); even once significant decreases in response to white light are observed in *Prph2*$^{+/-}$ animals. Surprisingly, we observed fairly substantial photopic ERG responses in the *Prph2*$^{K\Delta/K\Delta}$ at P30 compared to *Prph2*$^{-/-}$ (Fig. 3A and B), but this function was below the signal to noise ratio by 4 months of age so these animals were not included in long-term aging studies.

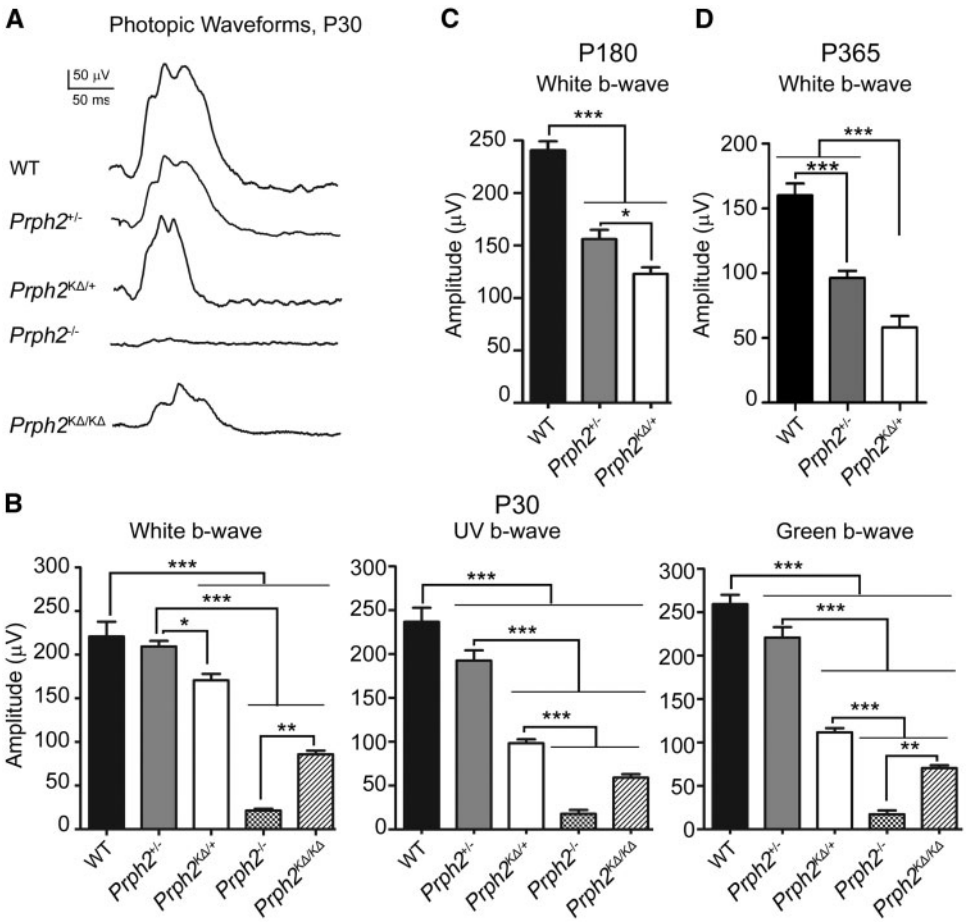

Figure 3. K153Δ Prph2 leads to defects in cone function. Full-field ERGs were recorded under photopic conditions. **(A)** Representative P30 photopic waveforms are shown from all genotypes. **(B–D)** Plotted are mean (±SEM) maximum photopic b-wave amplitudes recorded under white light, UV light, or green light at P30 **(B)**, P180 **(C)**, or P365 **(D)**. $^{*}P < 0.05$ $^{***}P < 0.001$ in one-way ANOVA with Bonferroni's post-hoc comparison.

K153Δ Prph2 led to funduscopic abnormalities consistent with patients' phenotypes

In addition to RP, patients with the K153Δ mutation can also present with macular dystrophies including PD. One of the features of PD is characteristic funduscopic changes that occur due to defects in the choroid and retinal pigment epithelium (RPE), and accumulation of RPE lipofuscin. Consistent with the late age-of-onset of these phenotypes in patients, we observed no alterations in the fundus phenotype at P30 in K153Δ mice (Supplementary Material, Fig. S2). However, by P180, we begin to observe flecking in the *Prph2*$^{KΔ/+}$ retina (Fig. 4a, black arrows, top). This flecking is similar to but of lesser extent than that which we have previously observed in other *Prph2* PD mutations such as Y141C (19), and is not observed in age-matched *Prph2*$^{+/-}$ and WT eyes. This speckling is more severe in the *Prph2*$^{KΔ/KΔ}$, and also occurs to a lesser degree in the *Prph2*$^{-/-}$eyes. Retinal vasculature as assessed by fluorescein angiography is largely normal at P180 in all genotypes (Fig. 4a, bottom). At P365, the yellow flecking in the *Prph2*$^{KΔ/+}$ does not worsen, and the flecking in the *Prph2*$^{-/-}$ and *Prph2*$^{KΔ/KΔ}$ attenuates in favour of large splotches (Fig. 4B, arrowheads) which often align with leaky areas on fluorescein angiograms (Fig. 4B, bottom). We have previously observed these splotches (19) and hypothesize that they arise due to the ongoing degeneration which is quite severe in the *Prph2*$^{-/-}$ by P365. Though the tissue of origin of the flecking apparent in the *Prph2*$^{KΔ/+}$ is not known, these data suggest that the K153Δ knockin line also models some aspects of the clinical phenotype seen in patients carrying this mutation.

K153Δ expressed on the *Nrl*$^{-/-}$ background leads to defects in cone structure and function

Thus far we have observed that the K153Δ mutant allele is largely non-functional with some potential dominant-negative effects on rod and cone function, but not rod structure. Further exploration of the cellular/biochemical underpinnings of cone effects is difficult since the WT retina is ∼95% rods. To further explore cone phenotypes, we crossed the K153Δ onto the cone-dominant *Nrl*$^{-/-}$ retina (20), which has been widely used for this purpose. We first validated that the cone-like photoreceptors of the *Nrl*$^{-/-}$ would respond to the K153Δ mutant allele similar to WT cones by conducting photopic ERG at P30 in *Prph2*$^{KΔ/+}$/*Nrl*$^{-/-}$ animals. We find that the photopic responses in the *Nrl*$^{-/-}$ largely recapitulate those from the WT, specifically the observation that photopic responses are worse in *Prph2*$^{KΔ/+}$/*Nrl*$^{-/-}$ than in *Prph2*$^{+/-}$/*Nrl*$^{-/-}$ (Fig. 5A). The *Nrl*$^{-/-}$ retina is characterized by rosettes in the ONL (Fig. 5B, R), so morphometric analyses are difficult. However, examination at the TEM level can provide insight into cone OS ultrastructure. Cone OSs in the *Prph2*$^{+/-}$/*Nrl*$^{-/-}$ adopt a whorl-like morphology

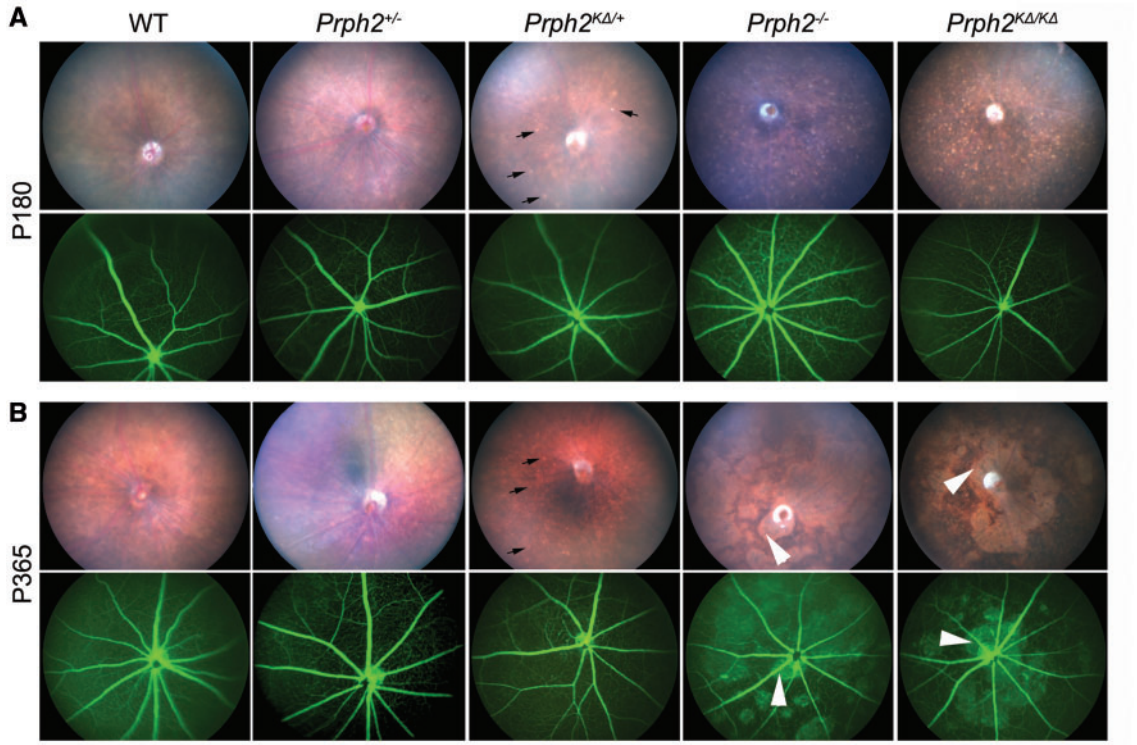

Figure 4. K153Δ leads to fundus flecking characteristic of PD. **(A–B)** Funduscopic examination was performed at the indicated genotype at P180 (**A**) and at P365 (**B**). Shown are representative brightfield fundus images (top) and fluorescein angiograms (bottom). Arrows indicate flecking phenotype found in the *Prph2*$^{K\Delta/+}$ as well as the *Prph2*$^{-/-}$ and *Prph2*$^{K\Delta/K\Delta}$. Arrowheads indicate splotching, likely due to severe photoreceptor degeneration, which occurs at later ages. $n = 6$-8 eyes/group.

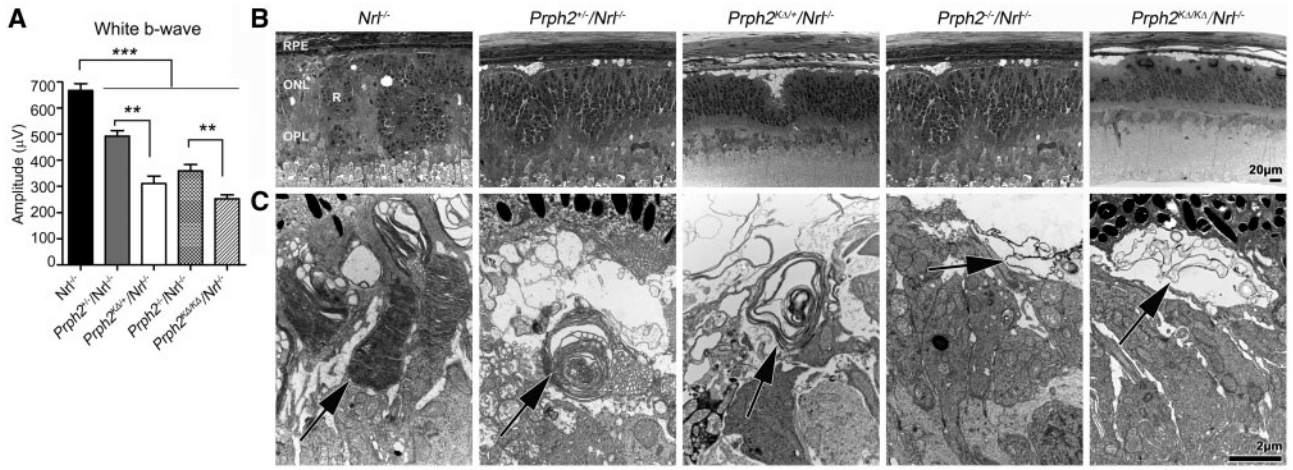

Figure 5. Expression of K153Δ on the *Nrl*$^{-/-}$ background leads to deficits in cone structure and function. **(A)** Full-field ERGs were recorded from all listed genotypes under photopic conditions at P30. Mean (±SEM) maximum photopic b-waves in response to white light are plotted. $^{*}P < 0.05$, $^{**}P < 0.01$, $^{***}P < 0.001$ by one-way ANOVA with Bonferroni's post-hoc comparison. **(B–C)** Shown are representative light microscopy (**B**) and transmission EM images (**C**) from the indicated genotypes at P30. RPE: retinal pigment epithelium, ONL: outer nuclear layer, OPL: outer plexiform layer, R: rosette. Scale bars 20 μm (light microscopy), 2 μm (EM).

similar to *Prph2*$^{+/-}$ rods, while *Prph2*$^{-/-}$/*Nrl*$^{-/-}$ cones exhibit open balloon like OSs which lack lamellae but nevertheless retain function (18,21). In contrast to the case with rods, we find no improvements in cone OS ultrastructure in the *Prph2*$^{K\Delta/+}$/*Nrl*$^{-/-}$ versus *Prph2*$^{+/-}$/*Nrl*$^{-/-}$ (Fig. 5C, arrows indicate OSs), and many cones exhibit worsened ultrastructure. The phenotype in the *Prph2*$^{K\Delta/+}$/*Nrl*$^{-/-}$ is largely in between that in the *Prph2*$^{+/-}$/*Nrl*$^{-/-}$and that in the *Prph2*$^{-/-}$/*Nrl*$^{-/-}$; some cones in the *Prph2*$^{K\Delta/+}$/*Nrl*$^{-/-}$ exhibited a few whorl-like OSs (as pictured in Fig. 5C), but many exhibited open, sac-like OSs without lamellae or whorls (Supplementary Material, Fig. S3).

K153Δ differentially affects complex assembly in rods versus cones

Assembly of covalent and non-covalently linked homo- and heteromeric complexes between Prph2 and Rom1 is critical for

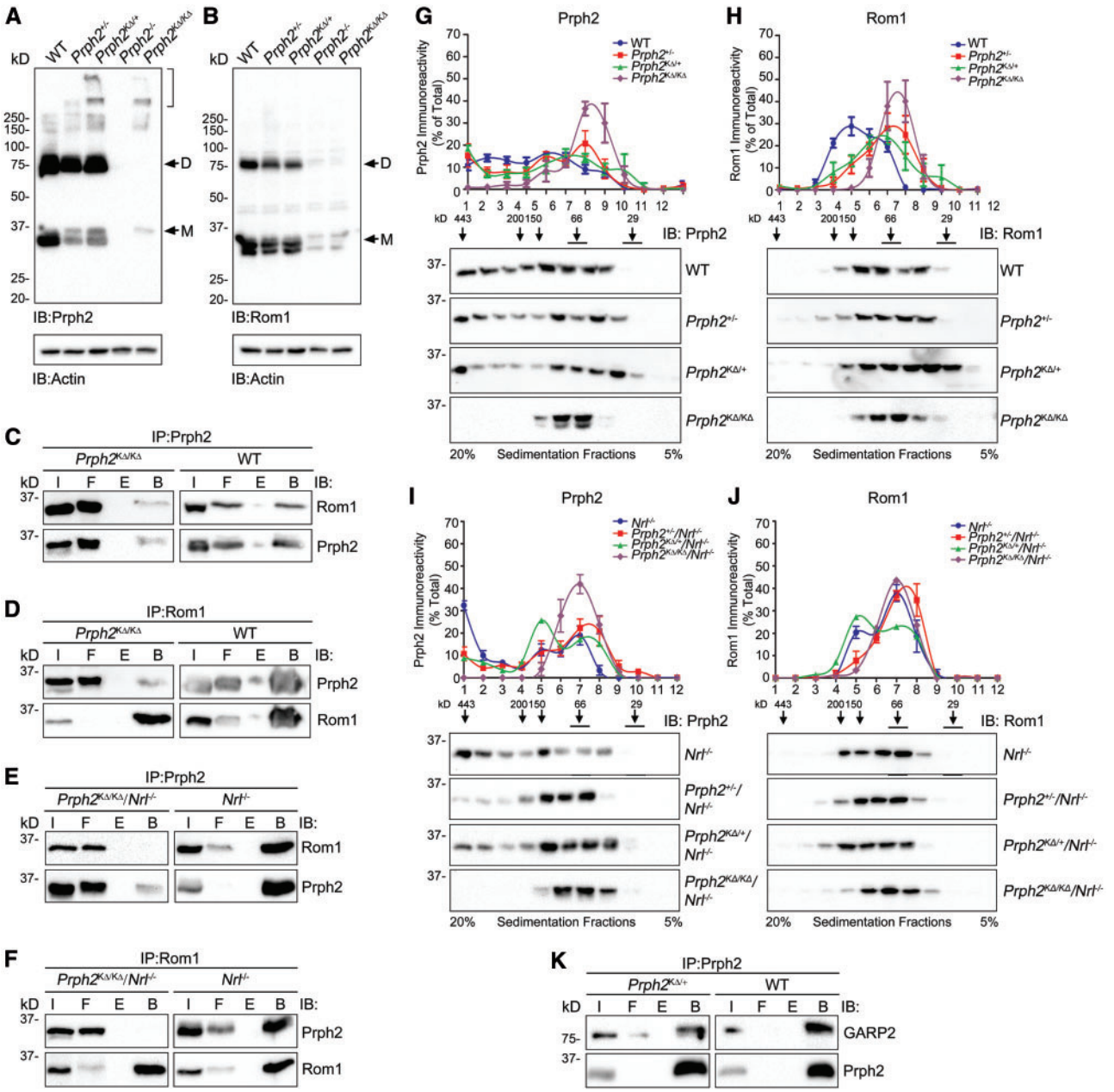

Figure 6. K153Δ causes abnormalities in complex formation. **(A–B)** Non-reducing SDS-PAGE/western blot were performed on P30 retinal extracts in the presence of n-ethyl maleimide (to prevent post-extraction cysteine shuffling) and probed with antibodies against Prph2 (**A**), Rom1 (**B**) and actin. Prph2/Rom1 monomers and dimers are represented by the M/D, respectively. Bracket highlights aggregation in extracts from animals containing the K153Δ allele. **(C–F)**. Reciprocal co-immunoprecipitation was performed using the antibodies indicated at the top of each panel. Resultant reducing SDS-PAGE/western blots were probed with either Prph2 or Rom1. I: input, F: flow-through (unbound), B: bound, E: empty. **(G–J).** P30 retinal extracts were prepared from the indicated genotype and separated on a continuous 20% to 5% non-reducing sucrose gradient. Fractions were collected and analyzed using reducing SDS–PAGE/western blot using antibodies specific for Prph2 **(G, I)** and Rom1 **(H, J)**. The positions of standard molecular weight markers are indicated above representative blots using the same protocol published previously (4). Graphs plot the percent of total Prph2 or Rom1 found in each fraction (mean ±SEM). **(K)** Retinal extracts underwent cross-linking followed by IP for Prph2. Resultant blots were probed for Prph2 or GARP. N= 3–6 independent experiments/genotype.

their function. Our previous data have suggested that complex assembly is different in rods and cones and may be inversely affected by different mutations (3,10,22). Prph2 higher-order and intermediate complexes are assembled from tetramers via intermolecular covalent linkages mediated by C150, and run as dimers under denaturing but non-reducing conditions. Given the proximity of the K153Δ mutation to C150, we asked whether K153Δ has any effect onPrph2 dimer formation. Non-reducing SDS-PAGE/western blot showed that in *Prph2*$^{K\Delta/K\Delta}$, no Prph2 dimers are formed (Fig. 6A, D/M indicate dimers and monomers, respectively). However, in the *Prph2*$^{K\Delta/K\Delta}$, Rom1 continues to form a small amount of covalently-linked dimers (Fig. 6B). In the WT retina, Rom1 forms dimers largely with Prph2 (23), but it can also form homo-dimers which is likely what is present in the *Prph2*$^{K\Delta/K\Delta}$. Likewise in the *Nrl*$^{-/-}$ background, K153Δ protein alone did not form intermolecular disulphide linkages, and the

Rom1 dimer band was extremely faint (Supplementary Material, Fig. S4A). We also observed a trail of partial aggregation of Prph2 (Fig. 6a, bracket), but not Rom1, in animals carrying the K153Δ mutant allele, suggesting additional defects in protein folding or complex assembly may be present apart from defects in dimer assembly.

The C150S mutation interrupts covalent linkages and impairs Rom1/Prph2 interactions specifically in cones (3). To investigate whether the K153Δ mutation affects its interactions with wild-type Prph2 and Rom1, we performed reciprocal co-immunoprecipitation (IP) using Prph2 and Rom1 antibodies. Our IPs are not quantitative, but they do allow us to ask whether these interactions are preserved. In the WT background, Prph2 can pull-down Rom1 and vice versa (Fig. 6C–D). This finding is recapitulated in the $Prph2^{K\Delta/K\Delta}$, suggesting that K153Δ protein can bind Rom1 in rods (Fig. 6C–D). In striking contrast, in the $Prph2^{K\Delta/K\Delta}$ on the $Nrl^{-/-}$ background, no Rom1 was pulled down with in Prph2 IPs (Fig. 6E) and no Prph2 was pulled down in Rom1 IPs (Fig. 6F), suggesting that Rom1 in cones does not bind to K153Δ protein.

We next evaluated Prph2 and Rom1 oligomerization by velocity sedimentation which enables separation of different size complexes (3,4). Retinal extracts were fractionated on continuous 5%-20% non-reducing sucrose gradients and then separated on reducing SDS-PAGE. Western blots were probed with antibodies for Prph2 (Fig. 6G and I) and Rom1 (Fig. 6H and J), and the percent of total Prph2 or Rom1 in each gradient fraction was plotted. In the WT retina, Prph2 is presented as tetramers (fractions 6–8), intermediate oligomers (fractions 4–5) and higher order oligomers (fractions 1–3), while Rom1 is detected only in tetramers and intermediate oligomers. No significant alterations were observed in the distribution of Prph2 in its various complexes in the $Prph2^{K\Delta/+}$or $Prph2^{+/-}$compared to WT (Fig. 6G). However, in the $Prph2^{K\Delta/K\Delta}$ retinas, only tetrameric Prph2 was present; no intermediate or higher-order complexes were detected (Fig. 6G, purple). The pattern of Rom1 complexes in the $Prph2^{K\Delta/K\Delta}$ retinas is also shifted towards tetramers (Fig. 6H, purple) compared to WT (blue). This is consistent with the idea that covalent interactions between Prph2 and Rom1 (which are eliminated in the presence of the K153Δ mutation) mediate the assembly of Rom1 intermediate complexes, and thus though Rom1 is not mutated in $Prph2^{K\Delta/K\Delta}$ retinas; it fails to incorporate into intermediate complexes. The lack of covalent linkages in $Prph2^{K\Delta/K\Delta}$ tetramers can be seen when non-reducing gradient fractions are separated by SDS-PAGE under non-reducing conditions (Supplementary Material, Fig. S4B). Interestingly, both $Prph2^{K\Delta/+}$ and $Prph2^{+/-}$ exhibit an intermediate Rom1 complex assembly phenotype, with a shift towards tetramers at the expense of intermediate complexes (Fig. 6H) but not to the same degree as the $Prph2^{K\Delta/K\Delta}$. This phenotype may be due to the altered OS structure in the haploinsufficient $Prph2^{+/-}$ or because the ratio of WT Prph2 to Rom1 is altered in both genotypes. Combined, these data indicate that in the WT background, K153Δ Prph2 alone cannot form higher order complexes, but that when WT Prph2 is present, K153Δ does not adversely affect the distribution of Prph2 complex types.

To determine whether a complex assembly is differently affected by the K153Δ mutation in cones, gradient analysis was performed on retinas in the $Nrl^{-/-}$ background (Fig. 6I–J). As in the WT background, Prph2 and Rom1 were limited to tetrameric fractions in the $Prph2^{K\Delta/K\Delta}/Nrl^{-/-}$ (Fig. 6I–J, purple). Both the $Prph2^{+/-}/Nrl^{-/-}$ and the $Prph2^{K\Delta/+}/Nrl^{-/-}$retinas have a decrease in the amount of Prph2 found in the heaviest fractions (Fig. 6I). In addition, in the $Prph2^{K\Delta/+}/Nrl^{-/-}$ but not the $Prph2^{+/-}/Nrl^{-/-}$ there is increased formation of intermediate sized Prph2 and Rom1 complexes (Fig. 6I–J, green). These data indicate that there are subtle differences in complex assembly in cones in $Prph2^{+/-}/Nrl^{-/-}$versus $Prph2^{K\Delta/+}/Nrl^{-/-}$, and these differences may be due to the lack of binding between K153Δ Prph2 and Rom1 in cones.

Rom1 is Prph2's primary binding partner, but Prph2 also interacts with the retinal gene products of the *Cngb1* gene. These include the beta subunit of the rod cyclic nucleotide gated channel as well as the non-membrane-bound isoform GARP2 (glutamic acid rich protein) (24,25). This interaction is hypothesized to play a structural role in linking the plasma membrane and the disc rim as well as a potential functional role in organizing proteins for optimal phototransduction (24–26). We asked whether this interaction was abolished in the presence of the K153Δ allele. We conducted IP on cross-linked retinal extracts (as previously described (24)), and found that Prph2 interacts with GARP2 in both the WT and $Prph2^{K\Delta/+}$retina (Fig. 6K). This suggests that although the presence of K153Δ-Prph2 has negative effects on the Prph2/Rom1 complex formation, it does not abolish Prph2/GARP2 interactions. GARP2/CNGB1 are undetectable in the $Prph2^{-/-}$ (26), a finding recapitulated in the $Prph2^{K\Delta/K\Delta}$ retina (Supplementary Material, Fig. S4C), so we were unable to directly evaluate whether the K153Δ protein interacts with GARP2.

K153Δ Prph2 can traffic to the OS but also accumulates in the ONL

The OS trafficking signal for Prph2 is present in its C-terminus (27), however, mutations in the D2 loop can lead to abnormalities in OS targeting in cones (10). To evaluate whether the mutant K153Δ Prph2 properly localized to OSs, we performed immunofluorescence on P30 retinal sections using Prph2 (red) and Rom1, rhodopsin, S-opsin, or M-opsin (all in green, Fig. 7A). In the $Prph2^{K\Delta/+}$, Prph2 and Rom1 were both restricted to the OS layer, but we observed a small amount of mislocalization of rhodopsin and M-opsin (arrowheads, Fig. 7A) in the ONL and outer plexiform layers. To better visualize this, higher magnification images are shown in Supplementary Material, Fig. S5. In the $Prph2^{K\Delta/K\Delta}$, both Prph2 and rhodopsin, but not Rom1, are mislocalized throughout the ONL (brackets, Fig. 7A). Because the OSs are so small in the $Prph2^{K\Delta/K\Delta}$, it was difficult to determine on the light level whether the proteins of interest were actually located in the OSs or were found only at the ciliary tip (in the case of Rom1) or the IS/cell body (for rhodopsin and Prph2). Therefore, we conducted immunogold labeling coupled with EM imaging. All analysed proteins in the $Prph2^{K\Delta/+}$demonstrated immunogold labeling in the OSs (Fig. 7B, top). We likewise observed Prph2, Rom1, rhodopsin, and S-opsin immunogold labelling in the small OSs of the $Prph2^{K\Delta/K\Delta}$, suggesting that while a large amount of Prph2 and rhodopsin mislocalized throughout the cell, some made it to the nascent OSs.

Gene supplementation is of limited efficacy for the K153Δ mutation

The level of Prph2 expression has been shown to be critical for OS structure and function, particularly for rods, which are severely affected by haploinsufficiency. Thus, gene supplementation has been considered as a treatment approach for *Prph2*-associated disease, and has been effective for RP models (16,28,29). However, there is some question about whether gene

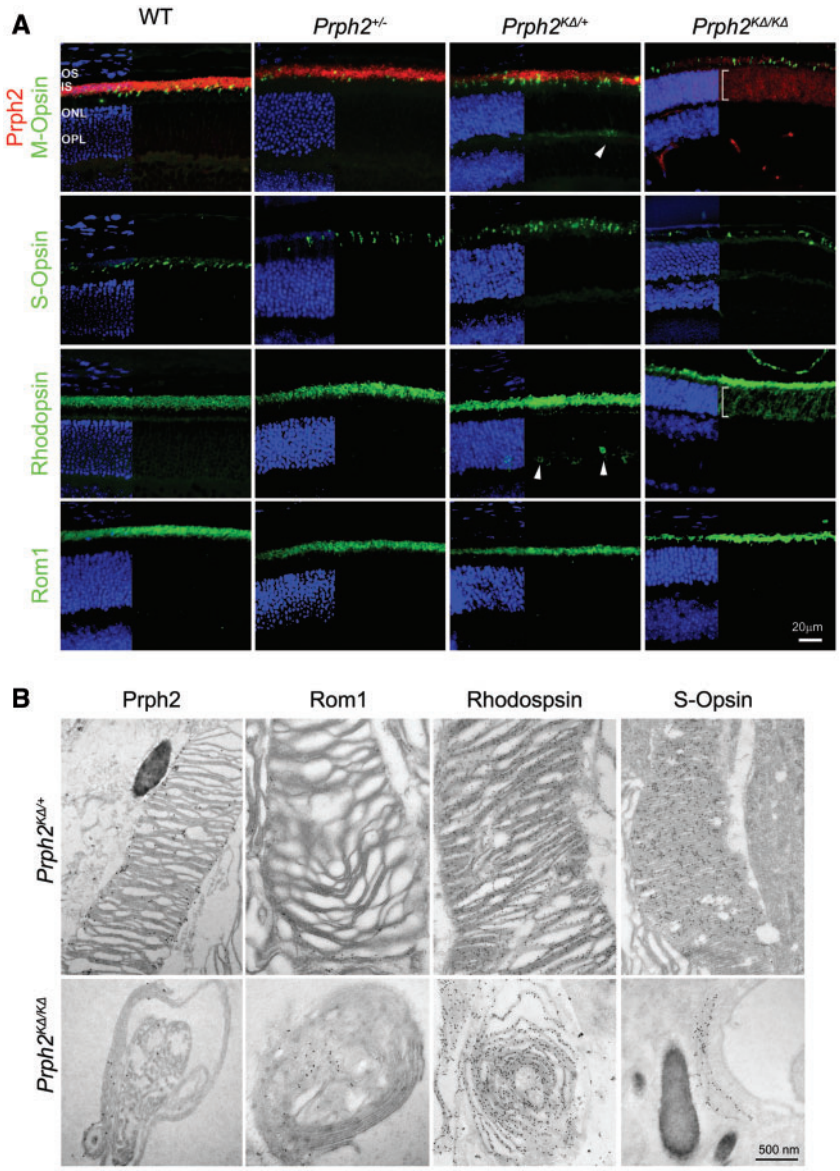

Figure 7. K153Δ-Prph2 traffics to the OS but also accumulates in the ONL. **(A)** Retinal sections from indicated genotypes were labeled with Prph2 (red) and Rom1, Rhodopsin, S-opsin, and M-opsin (green) at P30. Nuclei in all sections were counterstained with DAPI (blue). Arrowheads show minor mislocalization of rhodopsin and M-opsin in the $Prph2^{K\Delta/+}$. Brackets show wide ONL mislocalization. **(B)** Immunogold labeling with antibodies for Prph2, Rom1, rhodopsin and S-opsin, coupled with transmission EM was performed from the indicated genotypes at P30. Scale bars, 20 μM (light microscopy), 500 nm (EM). OS: outer segments, ONL: outer nuclear layer.

supplementation would be an effective approach for mutations such as K153Δ which combine haploinsufficiency-associated defects with apparent dominant-negative defects. To test the feasibility of gene supplementation, we took the advantage of our transgenic mouse model that overexpresses WT Prph2 (normal mouse peripherin [NMP]) (16). This transgene is driven by the human interphotoreceptor retinoid binding protein (IRBP) promoter which expresses in both rods and cones. One NMP allele results in transgenic Prph2 protein levels which are ~30% of WT levels (16), and NMP expression rescued the $Prph2^{+/-}$ structural and functional phenotype.

Here, we generated and evaluated the NMP/$Prph2^{K\Delta/+}$. In NMP/$Prph2^{K\Delta/+}$ retinas, western blot shows that levels of Prph2, Rom1 and rhodopsin were completely rescued to WT levels (Fig. 8A). However, though Prph2, Rom1, and rhodopsin protein levels were rescued, we observed only small improvements in scotopic ERG function at P30. Scotopic ERG in NMP/$Prph2^{K\Delta/+}$ did not exceed the severely haploinsufficient $Prph2^{+/-}$ (Fig. 8B, left and middle), much less attain WT levels. This is in striking contrast to the NMP/$Prph2^{+/-}$, which exhibited significant rescue of rod function in comparison to $Prph2^{+/-}$ (Fig. 8B left and middle,). A similar finding was observed in P30 photopic amplitudes; mean values in the NMP/$Prph2^{K\Delta/+}$ were slightly higher than those in the $Prph2^{K\Delta/+}$ but the difference did not achieve statistical significance (Fig. 8B, right). By P180 what little benefit there was from the NMP transgene in $Prph2^{K\Delta/+}$ animals had vanished, and there were no significant improvements in scotopic or photopic ERG in NMP animals compared to non-transgenic controls (Fig. 8C), again unlike the NMP/$Prph2^{+/-}$ in which rescue persisted at P180. In contrast to the lack of NMP-

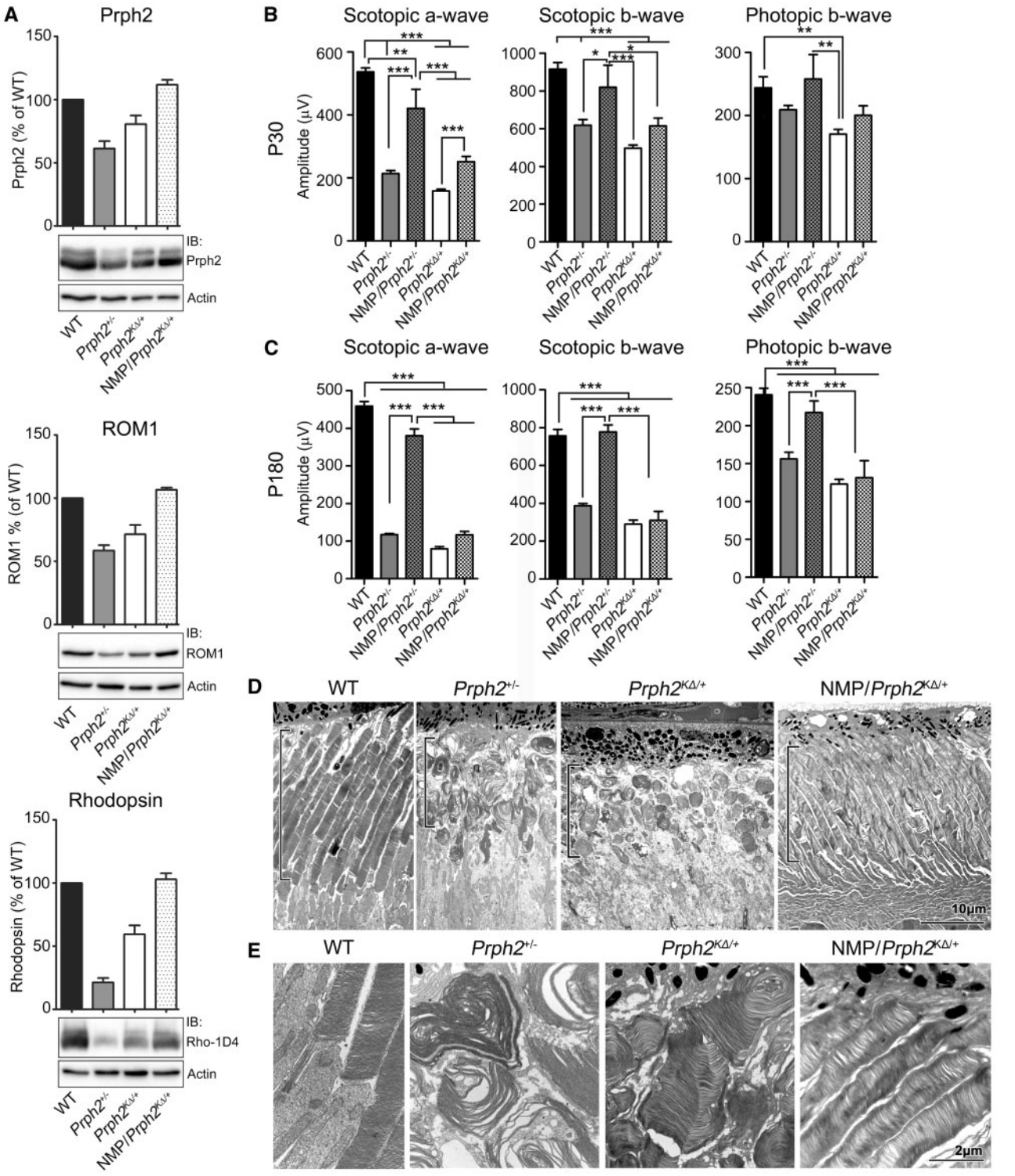

Figure 8. Supplementation with wild-type Prph2 does not rescue rod or cone function in *Prph2*$^{K\Delta/+}$. **(A)** Western blot analysis and quantification of Prph2, Rom1, rhodopsin and corresponding actin loading control are presented. **(B–C)** Amplitudes of scotopic a-wave, scotopic b-wave and photopic b-wave are shown from P30 **(B)** and P180 **(C)** of the indicated genotypes. **(D–E)** EM images are taken from P30 retinas of the indicated genotypes. Black brackets show OS length. Images in **(E)** are higher magnification of same genotypes as **(D)**. Scale bars, 10 μm **(D)**, 2 μm **(E)**.

mediated functional improvement in *Prph2*$^{K\Delta/+}$, rod ultrastructure was improved in NMP/*Prph2*$^{K\Delta/+}$ animals compared to *Prph2*$^{+/-}$ and *Prph2*$^{K\Delta/+}$ animals at P30 (Fig. 8D–E). Though we have insufficient samples to quantify, the overall length and arrangement of OSs is better in NMP/*Prph2*$^{K\Delta/+}$ than controls (black brackets in Fig. 8D highlight the OS layer). Similarly, OS disc stacking and alignment was almost as good in the NMP/*Prph2*$^{K\Delta/+}$ as in the WT (Fig. 8E).

Discussion

Prph2 and Rom1 rely on precise complex assembly mediated by both covalent and non-covalent bonds to function properly. Both our group and others have documented the critical role of C150 in Prph2 complex assembly and Prph2-mediated OS biogenesis (3,5,10), for example our studies of C150S transgenic mice. In spite of the clear importance of this residue, however, C150 is not a known site for pathological Prph2 mutations. Interestingly, our data here suggest that the K153Δ mutation largely mimics many aspects of the widely documented phenotypes of the C150S mutation. Specifically, we observe dominant functional defects in K153Δ cones, impaired binding of K153Δ to Rom1 in cones, and most strikingly, an inability of K153Δ Prph2 to form disulphide-linked higher order complexes, resulting in the formation of only Prph2 tetramers in *Prph2*$^{K\Delta/K\Delta}$ retinas. Interestingly, not all K153Δ phenotypes parallel those observed in C150S transgenics. Whether this is due to limitations of the transgenic approach or due to additional defects caused by the K153Δ is not clear, but in keeping with the occurrence of both rod and cone phenotypes in patients, the K153Δ mutation causes functional and trafficking defects in rods (further discussed below) which were not seen in C150S transgenics (3).

Previously, we showed that in the presence of WT Prph2, C150S in cones was mislocalized throughout the photoreceptor (3). This mislocalization was not observed in C150S rods. We attributed this variation to differences in the assembly of Prph2 complexes in rods versus cones, possibly arising due to the fact that C150S Prph2 (like K153Δ Prph2) can bind Rom1 in rods but not in cones. It is not clear why K153Δ Prph2 mistraffics in all photoreceptors, although it may be also tied to complex formation since we only observe severe mislocalization in the absence of WT Prph2, and thus only K153Δ Prph2 tetramers are present. It has been shown in *Xenopus* that most Prph2 traffics to the OS by a non-conventional secretory pathway which bypasses the trans-Golgi (30). In mouse retina, we have recently reported that tetrameric Prph2 largely traffics through a conventional secretory pathway, while the higher-order Prph2 oligomers traffic through the unconventional secretory pathway (31). Thus, it is likely that the K153Δ Prph2 that we observe in the OS (by immunogold) is the small fraction that would normally traffic through the conventional pathway, while the unconventional pathway remains unavailable to K153Δ (in the absence of WT) because it cannot assemble into large oligomers. In addition to Prph2 mislocalization, we also observe widespread rhodopsin mislocalization in the *Prph2*$^{K\Delta/K\Delta}$. Previously, we have observed this phenomenon in the *Prph2*$^{-/-}$, and concluded that without OSs, rhodopsin accumulates by default in the IS/ONL. Though there are some OS structures in the *Prph2*$^{K\Delta/K\Delta}$, they are quite small, and we hypothesize that rhodopsin mislocalization occurs for the same reason in the *Prph2*$^{K\Delta/K\Delta}$ as in the *Prph2*$^{-/-}$.

Here, we find that in contrast to many Prph2 RP mutants, such as C214S (32), which act as loss-of-function alleles and cause disease due to simple haploinsufficiency, the K153Δ allele exerts a dominant effect, worsening both rod and cone function (i.e. *Prph2*$^{+/-}$ is better than *Prph2*$^{K\Delta/+}$). It is difficult to distinguish whether this is due to dominant negative or gain-of-function effects. Some Prph2 mutations, such as P216L, clearly act as dominant negative alleles. The presence of the mutant leads to degradation of both mutant and WT protein, and results in early-onset RP due to severe haploinsufficiency (33). However, in other cases such as R172W and Y141C, both the mutant and WT Prph2 proteins are stable (19,22,34), yet defects in rod and/or cone structure and function occur, leading to the conclusion that the phenotypes are due to gain-of-function effects of the mutant allele. In the case of K153Δ, our finding that in the absence of WT Prph2, K153Δ protein is expressed at only 20% of WT levels (in spite of normal message levels) suggests that the K153Δ protein is unstable. Yet Prph2 protein levels in the *Prph2*$^{K\Delta/+}$are higher than *Prph2*$^{+/-}$ so the presence of one allele of K153Δ Prph2 is not likely affecting the stability of WT Prph2. Thus, it seems likely that the K153Δ has at least some toxic gain-of-function effects in rods and cones. This is a novel finding, as all other previously identified Prph2 mutations with gain-of-function effects have largely targeted cones rather than rods and cones.

Interestingly, however, the dominant disease mechanism for K153Δ may not be same in rods and cones, a phenomenon also seen for other proteins which are expressed in both cell types (35). For example, while the presence of the K153Δ allele worsens both rod and cone function (i.e. *Prph2*$^{+/-}$ is better than *Prph2*$^{K\Delta/+}$), it improves the rod structure while worsening cone structure. This disconnect in rod structure-function is likewise seen in experiments overexpressing WT Prph2. NMP/*Prph2*$^{K\Delta/+}$ retinas exhibit substantial improvements in rod OS ultrastructure without concurrent improvements in rod function. It was possible that this disconnect arose due to impairments in interactions between Prph2 and GARP2, but our data show that Prph2 continues to interact with GARP2 in the *Prph2*$^{K\Delta/+}$. These data suggest that K153Δ Prph2 may very well be able to partially support rod OS morphogenesis (provided WT Prph2 is present), but not necessarily support OS function. The divergent roles of Prph2 as a structural component critical for the formation of OSs and an OS functional component have recently been of interest. Prph2 and Rom1 are both tetraspanins, proteins that are known to organize membrane domains to promote cellular signalling. Thus, it has been hypothesized that Prph2 has a role as a protein critical for organizing functional protein domains at the OS disc rim/plasma membrane for optimal visual signalling apart from any role in promoting OS assembly. Prph2 is known to interact with several components critical to phototransduction, including the rod cyclic nucleotide gated channel beta subunit (CNGB1), the cytosolic isoforms of CNGB1 called GARPs (24,25), rhodopsin (36), and cone opsins (37). Furthermore, the *Prph2* cone-dominant macular dystrophy mutation V268I (38) has been shown to specifically affect Prph2 binding to M-opsin but not S-opsin or rhodopsin, supporting the idea that Prph2 may play a key role in organizing functional protein domains and that disease mutations may adversely affect these functional domains. Our data here suggest that in rods K153Δ may in fact impair this functional role of Prph2 without eliminating its ability to support the OS structure.

In contrast, functional defects in K153Δ cones seem to parallel structural defects. Though the reason for this divergence in rod versus cone outcomes is not clear, we have previously studied Prph2 mutations which likewise cause defects in a cone structure but have no effect (or even a beneficial effect) on the rod structure (22,34), and defects in other proteins expressed in rods and cones, such as RPGR, can differentially impact rods vs. cones and have different disease mechanisms in the two cell types (35). In the case of Prph2, this may be due to the finding that Prph2 appears to play a differential role in rod versus cone morphogenesis. Previous work suggests that Prph2-mediated rim formation acts as the initiating step in disc formation in rods (preceding the growth of discs via the incorporation of rhodopsin containing membrane), but is a secondary step in cones (i.e. rim formation follows the growth of S-opsin containing membrane) (17,39). In addition, Prph2 does not bind to the cone

CNG channel (40). This potentially different mechanism for K153Δ-associated defects in rods versus cones may significantly contribute to the inter- and intra-familial phenotypic heterogeneity that characterizes patient phenotypes. Genetic or environmental factors, including mutations in *ROM1* (12), could have the potential to act as modifiers for *PRPH2* disease and may preferentially worsen structural or functional aspects of Prph2 and thus push patient phenotypes towards RP as opposed to macular dystrophy/PD and vice-versa.

Further exploration of these divergent functions of Prph2 and their ability to mediate RP versus MD-type phenotypes will certainly be a focus of future work. Such studies will be facilitated by our finding that even though mice lack a macula, the K153Δ knockin mice do exhibit some of the clinical phenotypes, such as fundus speckling, that characterize Prph2-associated PD. Interestingly, the K153Δ fundus phenotype is less severe than in other Prph2 PD mutations such as Y141C (19), highlighting the phenotypic variability from mutation to mutation. Prph2-associated macular dystrophy and PD are often accompanied by deleterious effects on tissues outside the photoreceptors including the choroid and RPE (41), and yellowish flecking on the fundus has been recognized to arise due to defects in the RPE, accumulation of lipofuscin in the RPE, and defects in the choroidal vasculature (42). The precise origin of the flecking we observe in the K153Δ animals is not known and long-term studies evaluating both this and other extra-photoreceptor phenotypes will be critical next steps.

Finally, one of our goals has been the development of effective gene therapies for *Prph2*-associated disease. Though Prph2 haploinsufficiency is amenable to rescue using gene supplementation, either by transgenesis (16), adeno-associated virus (28), or non-viral DNA nanoparticles (29,43), many *Prph2* mutations have dominant effects, making simple gene supplementation a questionable strategy. Gene supplementation via transgenesis promoted good short-term rescue for the R172W mutation (44), which causes early-onset gain-of-function defects specifically in cones (34). However, by later time-points, this benefit is lost. Here we find that even at early time-points, supplementation with WT Prph2 in the $Prph2^{K\Delta/+}$ cannot appreciably rescue functional defects, even though Prph2, Rom1, and rhodopsin protein levels are rescued to WT levels. These observations underscore the idea that gene supplementation may be a difficult strategy to feasibly implement for the treatment of rod- or cone-dominant Prph2-associated disease when the mutant allele has gain-of-function or dominant negative effects. Thus future therapeutic approaches may need to target the mutant allele or find other ways to promote improved photoreceptor function to attain clinical applicability.

Materials and Methods

Ethics statement and animal care and use

The local Institutional Animal Care and Use Committees (IACUC; University of Oklahoma Health Sciences Center, Oklahoma City, OK, USA and University of Houston, Houston, TX, USA) approved all animal use. Experiments also conformed to the guidelines of the Association for Research in Vision and Ophthalmology (Rockville, MD). The K153Δ-Prph2 knockin mice were generated by the inGenious Targeting Laboratory, Inc. (Ronkonkoma, NY, USA). A silent TTC > TTT mutation (to facilitate genotyping) and the AAA deletion (to create the K153Δ mutation) were introduced into exon 1. The LoxP/FRT-Neomycin selection cassette was inserted 383 bp downstream of exon 1 (in Prph2's large first intron). The final targeting construct was 14.3 kbp, and was linearized and electroporated into ES cells. ES cells were screened for the presence of the desired allele and positive clones were injected into C57BL/6 blastocysts and implanted. Chimeric founders were bred to identify mice with germ line transmission, and then bred to FLPeR expressing mice (Stock#003946, Jackson Labs, Bar Harbor, ME, USA) to remove the Neo cassette. The three base-pair deletion generating the K153Δ mutation and resultant knockin line was made using the same approach as previously described (19,23). PCR genotyping confirmed that these mice do not carry the *rd8* mutation. Mice heterozygous or homozygous for the naturally occurring Prph2 null allele, called *rds*, were used from our colony as controls and are here referred to as$Prph2^{+/-}$, and $Prph2^{-/-}$(Originally obtained from Dr. Neeraj Agarwal, National Eye Institute, Bethesda, MD). WT littermates were used from our colony, also as controls, after confirming that WT littermates from heterozygous knockin crosses exhibited similar retinal structure and function to the WT animals in our colony. $Nrl^{-/-}$ mice were used from our colony and were originally obtained from Dr. Anand Swaroop (National Eye Institute, Bethesda, MD). Animals were maintained in cyclic light (12 hours light, 12 hours dark, ~30 lux).

Western blot analysis, immunoprecipitation and velocity sedimentation

Various primary antibodies were used for western blotting, immunofluorescence, and immunogold EM and are summarized in Table 1. Western blot, immunoprecipitation, and velocity sedimentation were performed as described previously (3,4). Briefly, retinal extracts were solubilized in 100 µl of chilled (4°C) buffer [PBS pH 7.0 containing 1% triton-X 100, 5 mM EDTA, 5 mg/ml n-ethylmaleimide (NEM), and a standard protease inhibitor cocktail] per retina. Immunoprecipitation was performed using protein A beads and the RDS-CT antibody, or RDS mAB 2C1 cross-linked to sepharose beads, and 150 µg (for WT and $Nrl^{-/-}$) or 300 µg (for $Prph2^{K\Delta/K\Delta}$ and $Prph2^{K\Delta/K\Delta}/Nrl^{-/-}$) retinal extract per experiment. Retinas were incubated in 2 mM dithiobismaleimidoethane (DTME), 2 mM dithiobis (succinimidyl propionate) (DSP) in PBS for 2 hrs. Cross-linker was removed, retinas were washed in solubilization buffer and IP proceeded as described above. SDS-PAGE and western blot were performed using standard protocols under reducing conditions (with DTT) or non-reducing conditions (without DTT). Non-reducing velocity sedimentation was performed using continuous density gradients of 5-20% sucrose and 200 µg protein/sample. Densitometric quantification was performed on non-saturated blots using the Image Lab Software (Bio-Rad, Temecula, CA). In some cases blot intensities were turned up in figures to enable visualization of hard to see bands.

Electroretinography

Full-field ERGs were performed as previously described (22). Mice were dark adapted overnight prior to ERG. Subsequently, the animals were anaesthetized and eyes were dilated. ERGs were recorded an UTAS system (LKC, Gaithersburg, MD,USA). Scotopic ERGs were recorded with a strobe flash stimulus of 157 cd-s/m^2 followed by light adaptation for 5 minutes at 29.03 cd/m^2. Photopic responses were recorded from 25 averaged flashes at 157 cd-s/m^2 for white light, 12.5 cd-s/m^2 for green light (530 nm) and 0.79 cd-s/m^2 for UV light (365 nm).

Table 1. Antibodies used in this study

Antigen	Antibody	Species	Source	References
Prph2	RDS-CT	Rbt-PC	In house	(3,4)
Prph2	mAB 2B7	Ms-MC	In house	(22)
Rom1	ROM1-CT	Rbt-PC	In-house	(3,4)
Rom1	mAB 2H5	Ms-MC	In-house	(19,22)
Rhodopsin	mAB 1D4	Ms-MC	Dr. Robert Molday, University of British Columbia	(17,46)
S-opsin	S-opsin	Rbt-PC	In-house	(10)
S-opsin	OPN1SW (N-20)	Gt-PC	Santa Cruz Biotechnology, cat# sc-14363	(19)
S-opsin	S-opsin	Rbt-PC	Dr. Cheryl Craft, University of Southern California	
M-opsin	Opsin 1 (Medium Wave)	Rbt-PC	Novus Biologicals cat# 110-74730	
CNGB1/GARP1/2	mAB 4B1	Ms-MC	Dr. Robert Molday	(24,26)

Abbreviations; D2: second intradiscal loop of PRPH2; ERG: electroretinography; GARP2: glutamic acid rich protein; IP: immunoprecipitation; K153Δ: deletion of codon 153 in Prph2; NMP: normal mouse peripherin-2 transgene; NRL: neural retina leucine zipper; ONL: outer nuclear layer; P: postnatal day; PD: pattern dystrophy; PRPH2: peripherin 2, also known as RDS or retinal degeneration slow; ROM1: rod outer segment membrane protein 1; RP: retinitis pigmentosa; RPE: retinal pigment epithelium; WT: wild-type

Light and transmission electron microscopy and immunogold labelling

The methods used for tissue collection, processing, plastic-embedding, transmission electron microscopy, and immunogold labelling were described previously (3,18,32). Antibodies for immunogold were used at 1:10, and secondaries were anti-mouse or anti-rabbit conjugated to 10nm gold. Light microscopy was performed using 0.75 μm plastic embedded sections and images were captured at 40X magnification using a Zeiss microscope. To evaluate ONL thickness and OS length, images were captured from central superior and inferior regions containing the optic nerve head and at least three retinal sections from three different eyes/genotype were used. ONL and OS layer thickness were measured using Adobe Photoshop CS5.

Fundus imaging and fluorescein angiography

Fundus imaging and fluorescein angiography were performed using the Micron III and Micron IV systems (Phoenix Research Laboratories, Pleasanton, CA, USA) as previously described (45). Brightfield fundus images and fundus fluorescence images were collected first (from anaesthetized/dilated animals) and then the animals were injected intraperitoneally with 100 ml of 1% (w/v) fluorescein sodium (Sigma-Aldrich). FA images were captured using an excitation and emission filters of 486 and 436 nm, respectively. All images were captured using StreamPix software (Phoenix Research Labs).

Immunofluorescence labelling

Eyes were harvested, dissected, fixed and embedded as previously described for paraffin sectioning (3). Immunostaining was performed as described previously (3,10) using the primary antibodies described in the Table 1. Appropriate AlexaFluor conjugated secondary antibodies (Life Technologies, Grand Island, NY) were used at a dilution of 1:1000. Images were captured using Olympus BX-62 microscope equipped with a spinning disc confocal unit at 40x (air, 0.9 NA) or 100x (oil, 1.4 NA) objective. Images were stored and deconvolved (nearest neighbours paradigm) using Slidebook® version 5. All images shown are single planes from confocal stacks.

Statistical analysis

Graphs are presented as mean ± SEM. Differences between genotypes were assessed by 1-way ANOVA with Bonferroni's post-hoc pairwise comparisons. $P < 0.05$ was considered significant. $^{*}P < 0.05$, $^{**}P < 0.01$ and $^{***}P < 0.001$.

Supplementary Material

Supplementary Material is available at *HMG* online.

Acknowledgements

The authors would like to thank Barb Nagel, Marcellus Banworth, Maggie Mwoyosvi, and Justin Burnett for technical assistance. We would also like to thank Robert Molday, Cheryl Craft, Neeraj Agarwal, and Anand Swaroop for provision of reagents as indicated in the text.

Conflict of Interest Statement. None declared.

Funding

Funding for this project was provided by the National Eye Institute (EY010609 and EY018656, MIN) and the Oklahoma Center for the Advancement of Science and Technology (SMC).

References

1. Molday, R.S., Hicks, D. and Molday, L. (1987) Peripherin. A rim-specific membrane protein of rod outer segment discs. *Invest. Ophthalmol. Vis. Sci.*, **28**, 50–61.
2. Jansen, H.G. and Sanyal, S. (1984) Development and degeneration of retina in rds mutant mice: electron microscopy. *J. Comp. Neurol.*, **224**, 71–84.
3. Chakraborty, D., Ding, X.Q., Conley, S.M., Fliesler, S.J. and Naash, M.I. (2009) Differential requirements for retinal degeneration slow intermolecular disulfide-linked oligomerization in rods versus cones. *Hum. Mol. Genet.*, **18**, 797–808.
4. Chakraborty, D., Ding, X.Q., Fliesler, S.J. and Naash, M.I. (2008) Outer segment oligomerization of Rds: evidence from mouse models and subcellular fractionation. *Biochemistry*, **47**, 1144–1156.
5. Goldberg, A.F., Loewen, C.J. and Molday, R.S. (1998) Cysteine residues of photoreceptor peripherin/rds: role in subunit

assembly and autosomal dominant retinitis pigmentosa. *Biochemistry*, **37**, 680–685.
6. Goldberg, A.F. and Molday, R.S. (1996) Defective subunit assembly underlies a digenic form of retinitis pigmentosa linked to mutations in peripherin/rds and rom-1. *Proc. Natl. Acad. Sci. USA*, **93**, 13726–13730.
7. Goldberg, A.F. and Molday, R.S. (1996) Subunit composition of the peripherin/rds-rom-1 disk rim complex from rod photoreceptors: hydrodynamic evidence for a tetrameric quaternary structure. *Biochemistry*, **35**, 6144–6149.
8. Kajiwara, K., Berson, E.L. and Dryja, T.P. (1994) Digenic retinitis pigmentosa due to mutations at the unlinked peripherin/RDS and ROM1 loci. *Science*, **264**, 1604–1608.
9. Kajiwara, K., Hahn, L.B., Mukai, S., Travis, G.H., Berson, E.L. and Dryja, T.P. (1991) Mutations in the human retinal degeneration slow gene in autosomal dominant retinitis pigmentosa. *Nature*, **354**, 480–483.
10. Chakraborty, D., Conley, S.M., Stuck, M.W. and Naash, M.I. (2010) Differences in RDS trafficking, assembly and function in cones versus rods: insights from studies of C150S-RDS. *Hum. Mol. Genet.*, **19**, 4799–4812.
11. Clarke, G., Goldberg, A.F., Vidgen, D., Collins, L., Ploder, L., Schwarz, L., Molday, L.L., Rossant, J., Szel, A., Molday, R.S., *et al.* (2000) Rom-1 is required for rod photoreceptor viability and the regulation of disk morphogenesis. *Nat. Genet.*, **25**, 67–73.
12. Poloschek, C.M., Bach, M., Lagreze, W.A., Glaus, E., Lemke, J.R., Berger, W. and Neidhardt, J. (2010) ABCA4 and ROM1: implications for modification of the PRPH2-associated macular dystrophy phenotype. *Invest. Ophthalmol. Vis. Sci.*, **51**, 4253–4265.
13. Weleber, R.G., Carr, R.E., Murphey, W.H., Sheffield, V.C. and Stone, E.M. (1993) Phenotypic variation including retinitis pigmentosa, pattern dystrophy, and fundus flavimaculatus in a single family with a deletion of codon 153 or 154 of the peripherin/RDS gene. *Arch. Ophthalmol.*, **111**, 1531–1542.
14. Hawkins, R.K., Jansen, H.G. and Sanyal, S. (1985) Development and degeneration of retina in rds mutant mice: photoreceptor abnormalities in the heterozygotes. *Exp. Eye Res.*, **41**, 701–720.
15. Cheng, T., Peachey, N.S., Li, S., Goto, Y., Cao, Y. and Naash, M.I. (1997) The effect of peripherin/rds haploinsufficiency on rod and cone photoreceptors. *J. Neurosci.*, **17**, 8118–8128.
16. Nour, M., Ding, X.Q., Stricker, H., Fliesler, S.J. and Naash, M.I. (2004) Modulating expression of peripherin/rds in transgenic mice: critical levels and the effect of overexpression. *Invest. Ophthalmol. Vis. Sci.*, **45**, 2514–2521.
17. Chakraborty, D., Conley, S.M., Al-Ubaidi, M.R. and Naash, M.I. (2014) Initiation of rod outer segment disc formation requires RDS. *PLoS One*, **9**, e98939.
18. Farjo, R., Skaggs, J.S., Nagel, B.A., Quiambao, A.B., Nash, Z.A., Fliesler, S.J. and Naash, M.I. (2006) Retention of function without normal disc morphogenesis occurs in cone but not rod photoreceptors. *J. Cell Biol.*, **173**, 59–68.
19. Stuck, M.W., Conley, S.M. and Naash, M.I. (2014) The Y141C knockin mutation in RDS leads to complex phenotypes in the mouse. *Hum. Mol. Genet.*, **23**, 6260–6274.
20. Mears, A.J., Kondo, M., Swain, P.K., Takada, Y., Bush, R.A., Saunders, T.L., Sieving, P.A. and Swaroop, A. (2001) Nrl is required for rod photoreceptor development. *Nat. Genet.*, **29**, 447–452.
21. Farjo, R., Fliesler, S.J. and Naash, M.I. (2007) Effect of Rds abundance on cone outer segment morphogenesis, photoreceptor gene expression, and outer limiting membrane integrity. *J. Comp. Neurol.*, **504**, 619–630.
22. Conley, S.M., Stuck, M.W., Burnett, J.L., Chakraborty, D., Azadi, S., Fliesler, S.J. and Naash, M.I. (2014) Insights into the mechanisms of macular degeneration associated with the R172W mutation in RDS. *Hum. Mol. Genet.*, **23**, 3102–3114.
23. Stuck, M.W., Conley, S.M. and Naash, M.I. (2015) Retinal Degeneration Slow (RDS) Glycosylation Plays a Role in Cone Function and in the Regulation of RDS.ROM-1 Protein Complex Formation. *J. Biol. Chem.*, **290**, 27901–27913.
24. Poetsch, A., Molday, L.L. and Molday, R.S. (2001) The cGMP-gated channel and related glutamic acid-rich proteins interact with peripherin-2 at the rim region of rod photoreceptor disc membranes. *J. Biol. Chem.*, **276**, 48009–48016.
25. Ritter, L.M., Khattree, N., Tam, B., Moritz, O.L., Schmitz, F. and Goldberg, A.F. (2011) In situ visualization of protein interactions in sensory neurons: glutamic acid-rich proteins (GARPs) play differential roles for photoreceptor outer segment scaffolding. *J. Neurosci.*, **31**, 11231–11243.
26. Chakraborty, D., Conley, S.M., DeRamus, M.L., Pittler, S.J. and Naash, M.I. (2015) Varying the GARP2-to-RDS Ratio Leads to Defects in Rim Formation and Rod and Cone Function. *Invest. Ophthalmol. Vis. Sci.*, **56**, 8187–8198.
27. Tam, B.M., Moritz, O.L. and Papermaster, D.S. (2004) The C terminus of peripherin/rds participates in rod outer segment targeting and alignment of disk incisures. *Mol. Biol. Cell*, **15**, 2027–2037.
28. Ali, R.R., Sarra, G.M., Stephens, C., Alwis, M.D., Bainbridge, J.W., Munro, P.M., Fauser, S., Reichel, M.B., Kinnon, C., Hunt, D.M., *et al.* (2000) Restoration of photoreceptor ultrastructure and function in retinal degeneration slow mice by gene therapy. *Nat. Genet.*, **25**, 306–310.
29. Cai, X., Conley, S.M., Nash, Z., Fliesler, S.J., Cooper, M.J. and Naash, M.I. (2010) Gene delivery to mitotic and postmitotic photoreceptors via compacted DNA nanoparticles results in improved phenotype in a mouse model of retinitis pigmentosa. *Faseb J.*, **24**, 1178–1191.
30. Tian, G., Ropelewski, P., Nemet, I., Lee, R., Lodowski, K.H. and Imanishi, Y. (2014) An unconventional secretory pathway mediates the cilia targeting of peripherin/rds. *J. Neurosci.*, **34**, 992–1006.
31. Zulliger, R., Conley, S.M., Mwoyosvi, M.L., Stuck, M.W., Azadi, S. and Naash, M.I. (2015) SNAREs Interact with Retinal Degeneration Slow and Rod Outer Segment Membrane Protein-1 during Conventional and Unconventional Outer Segment Targeting. *PLoS One*, **10**, e0138508.
32. Stricker, H.M., Ding, X.Q., Quiambao, A., Fliesler, S.J. and Naash, M.I. (2005) The Cys214–>Ser mutation in peripherin/rds causes a loss-of-function phenotype in transgenic mice. *Biochem. J.*, **388**, 605–613.
33. Kedzierski, W., Lloyd, M., Birch, D.G., Bok, D. and Travis, G.H. (1997) Generation and analysis of transgenic mice expressing P216L-substituted rds/peripherin in rod photoreceptors. *Invest. Ophthalmol. Vis. Sci.*, **38**, 498–509.
34. Ding, X.Q., Nour, M., Ritter, L.M., Goldberg, A.F., Fliesler, S.J. and Naash, M.I. (2004) The R172W mutation in peripherin/rds causes a cone-rod dystrophy in transgenic mice. *Hum. Mol. Genet.*, **13**, 2075–2087.
35. Rao, K.N., Li, L., Zhang, W., Brush, R.S., Rajala, R.V. and Khanna, H. (2016) Loss of human disease protein retinitis pigmentosa GTPase regulator (RPGR) differentially affects rod or cone-enriched retina. *Hum. Mol. Genet.*, **25**, 1345–1356.
36. Becirovic, E., Nguyen, O.N., Paparizos, C., Butz, E.S., Stern-Schneider, G., Wolfrum, U., Hauck, S.M., Ueffing, M.,

Wahl-Schott, C., Michalakis, S., *et al.* (2014) Peripherin-2 couples rhodopsin to the CNG channel in outer segments of rod photoreceptors. *Hum. Mol. Genet.*, **23**, 5989–5997.
37. Nguyen, O.N., Bohm, S., Giessl, A., Butz, E.S., Wolfrum, U., Brandstatter, J.H., Wahl-Schott, C., Biel, M. and Becirovic, E. (2016) Peripherin-2 differentially interacts with cone opsins in outer segments of cone photoreceptors. *Hum. Mol. Genet.*, **25**, 2367–2377.
38. Felbor, U., Schilling, H. and Weber, B.H. (1997) Adult vitelliform macular dystrophy is frequently associated with mutations in the peripherin/RDS gene. *Hum. Mutat.*, **10**, 301–309.
39. Conley, S.M., Al-Ubaidi, M.R., Han, Z. and Naash, M.I. (2014) Rim formation is not a prerequisite for distribution of cone photoreceptor outer segment proteins. *FASEB J.*, **28**, 3468–3479.
40. Conley, S.M., Ding, X.Q. and Naash, M.I. (2010) RDS in Cones Does Not Interact with the Beta Subunit of the Cyclic Nucleotide Gated Channel. *Adv. Exp. Med. Biol.*, **664**, 63–70.
41. Boon, C.J., den Hollander, A.I., Hoyng, C.B., Cremers, F.P., Klevering, B.J. and Keunen, J.E. (2008) The spectrum of retinal dystrophies caused by mutations in the peripherin/RDS gene. *Prog. Retin. Eye Res.*, **27**, 213–235.
42. Francis, P.J., Schultz, D.W., Gregory, A.M., Schain, M.B., Barra, R., Majewski, J., Ott, J., Acott, T., Weleber, R.G. and Klein, M.L. (2005) Genetic and phenotypic heterogeneity in pattern dystrophy. *Br. J. Ophthalmol.*, **89**, 1115–1119.
43. Cai, X., Nash, Z., Conley, S.M., Fliesler, S.J., Cooper, M.J. and Naash, M.I. (2009) A partial structural and functional rescue of a retinitis pigmentosa model with compacted DNA nanoparticles. *PLoS One*, **4**, e5290.
44. Conley, S., Nour, M., Fliesler, S.J. and Naash, M.I. (2007) Late-onset cone photoreceptor degeneration induced by R172W mutation in Rds and partial rescue by gene supplementation. *Invest. Ophthalmol. Vis. Sci.*, **48**, 5397–5407.
45. Koirala, A., Makkia, R.S., Conley, S.M., Cooper, M.J. and Naash, M.I. (2013) S/MAR-containing DNA nanoparticles promote persistent RPE gene expression and improvement in RPE65-associated LCA. *Hum. Mol. Genet.*, **22**, 1632–1642.
46. MacKenzie, D., Arendt, A., Hargrave, P., McDowell, J.H. and Molday, R.S. (1984) Localization of binding sites for carboxyl terminal specific anti-rhodopsin monoclonal antibodies using synthetic peptides. *Biochemistry*, **23**, 6544–6549.